J Solid State Electrochem (2012) 16:25–33
DOI 10.1007/s10008-010-1262-y

ORIGINAL PAPER

Effect of annealing on the supercapacitor performance of CuO-PAA/CNT films

Jasmin S. Shaikh · Rajendra C. Pawar · Sawanta S. Mali · Annnasaheb V. Moholkar · J. H. Kim · Pramod S. Patil

Received: 24 September 2010 / Revised: 20 November 2010 / Accepted: 28 November 2010 / Published online: 22 December 2010

Abstract We report the synthesis of CuO-poly(acrylic) acid/CNT hybrid thin films by a cost-effective spin-coating technique for supercapacitor application. Hybrid films were annealed at 300, 400, and 500 °C to study its effect on the supercapacitor behavior. X-ray photoelectron spectroscopy and Fourier transform-infrared spectroscopy techniques were used for the phase identification and determination of the organic component in the hybrid films, respectively. Surface morphology of the films was examined by scanning electron microscopy and revealed the novel ring-like structures. The average diameter of the ring changes from 0.5 to 1.2 μm with increase in annealing temperature. Cyclic voltammetry is employed to estimate the specific capacitance (C_{sp}) of the films in 1 M H_2SO_4 electrolyte. It is observed that the C_{sp} increases from 188 to 258 Fg^{-1} with increase in annealing temperature.

Keywords Supercapacitor · Copper oxide (CuO) · Poly (acrylic) acid (PAA) · Carbon Nanotubes (CNTs)

Introduction

Supercapacitors (electrochemical capacitors) are used as uninterruptible power sources, can be coupled with batteries to provide peak power, and replace batteries for memory back-up [1–4]. It stores electrical energy in the electrode/electrolyte interface. Depending upon charge storage mechanism, it is divided into two categories—(1) electric double-layer capacitors (EDLC) and (2) pseudocapacitors. EDLC shows an electrostatic attraction with accumulation of charges at the electrode/electrolyte double-layer interfaces, while pseudocapacitors exhibit Faradic redox reactions. Materials like carbon nanotubes (CNTs), activated carbon, graphite etc. exhibit EDLC behavior [5–8], and metal oxides [9, 10] and conducting polymers [11–13] exhibit pseudocapacitance. In the development of the EDLC, CNTs are of particular interest because of their unique tubular porous structure, low electronic resistivity, chemical stability, low mass density, and large surface area, which facilitate fast ion and electron transportation. However, inherently low (C_{sp}) of the CNTs (15 to 80 Fg^{-1}) restricted their use as an electrode in supercapacitor devices [14, 15]. C_{sp} can be increased to ~130 Fg^{-1} by subsequent functionalization of CNTs and introduces additional surface functionality, which is capable of contributing to pseudocapacitance [14, 15].

One of the most critical aspects in the development of supercapacitor is to optimize the energy density without deteriorating their high power capability. Hybrids of EDLC and pseudocapacitor materials provide high C_{sp} and energy density [16]. CNTs with metal oxide show the improved stability and conductivity of the electrodes [16]. Ko et al. synthesized MnO_2/activated carbon nanotube composite by the coprecipitation method and the C_{sp} was estimated to be 250 Fg^{-1} at 10 mV/s in aqueous Na_2SO_4 solution. RuO_2/CNT composites recently achieved very high C_{sp} values over 1,000 Fg^{-1} [17].

CuO is an attractive candidate for supercapacitor electrode materials because it is environmentally benign,

J. S. Shaikh · R. C. Pawar · S. S. Mali · P. S. Patil (✉)
Thin Film Materials Laboratory, Department of Physics,
Shivaji University,
Kolhapur 416004, India
e-mail: psp_phy@unishivaji.ac.in

A. V. Moholkar · J. H. Kim
Department of Materials Science and Engineering,
Chonnam National University,
Gwangju, South Korea

cost-effective, and exhibits favorable pseudocapacitive characteristics. The highest reported C_{sp} value for the CuO in 1 M Na_2SO_4 was reported by Dubal et al., who synthesized CuO thin films having 1.2 μm thickness by chemical bath deposition method [18]. However, the C_{sp} is about 46 Fg^{-1} over limited potential window of ±0.1 to −0.7 V vs. saturated calomel electrode (SCE). One of the challenging issues in development of CuO-based high-performance supercapacitor is to improve its electronic conductivity, thereby yielding higher C_{sp}.

The pseudocapacitance behavior of the CuO and EDLC behavior together with the high conductivity of the CNTs coupled with the complex formation ability of poly(acrylic) acid (PAA) made us to choose the CuO-PAA/CNTs hybrid material for the supercapacitor electrode fabrication. The presence of the carboxylic group (COOH) in PAA improves the dispersibility of CNTs in water due to double functionalization [19–21]. An ability of CuO-PAA/CNT to exhibit supercapacitor behavior and upgradability of its C_{sp} with annealing temperature have been demonstrated.

Experimental details

Purification and functionalization of MWCNTs

Powdered multiwalled carbon nanotubes (MWCNTs; Monad Nanotech Pvt. Ltd., Mumbai, India) were purified and functionalized with –COOH by acid treatments. Briefly, 200 mg of MWCNTs were refluxed in the solution of concentrated H_2SO_4 (6 ml) and HNO_3 (2 ml). MWCNTs sediments were washed with distilled water several times and separated using a cooling centrifuge machine (REMI C24) at −5 °C for 15,000 rpm. Centrifuged MWCNTs were dried in vacuum furnace at 50 °C and designated as functionalized MWCNT–COOH.

Preparation of CuO-PAA and CuO-PAA/CNT hybrid films

The spin-coating technique was used to deposit the CuO-PAA and CuO-PAA/CNT films. Procedure given below is used to obtain hybrid films;

The CuO-PAA films were deposited by dissolving 0.1 g of $CuCl_2{\cdot}2H_2O$ (1 M) and 1.8 g of PAA (2 mM) in 9 ml of distilled water, which was subsequently stirred for 20 min using a magnetic stirrer (solution A). Solution A was spin coated on steel substrate at 3,000 rpm. The coated films were annealed at 500 °C and referred as CP_{500}. Further, to deposit CuO-PAA/CNT films, 0.002 g of MWCNT–COOH powder was added into the solution A, followed by 8 h stirring at room temperature. After stirring, ultrasonic treatment was given to this solution for 30 min to obtain stable dispersion of MWCNT–COOH in solution and is referred as solution B. Solution B was spin coated on steel substrate at 3,000 rpm to deposit CuO-PAA/CNT hybrid films. The coated films were annealed at 300, 400, and 500 °C, respectively, and deposited mass was found to be in the range between 0.1 and 0.2 mg per 1 cm^2. The films annealed at 300, 400, and 500 °C are denoted as $CPCNT_{300}$, $CPCNT_{400}$, and $CPCNT_{500}$.

X-ray photoelectron spectra were recorded using X-ray photoelectron spectroscopy (XPS), VG Multilab 2000, Thermo VG Scientific, UK, for phase evaluation. Fourier transform-infrared spectroscopy (FT-IR) was carried out on the PerkinElmer, model 783, USA, spectrometer to confirm the CuO-PAA/CNT chemical bonding. To record spectrograms pellet was prepared by mixing KBr with CuO-PAA/CNT powder in 300:1 proportion and then pressing the pellet between two pieces of polished steel. The optical absorption spectrum of the films was measured by ultraviolet-visible spectroscopy (Shimazdu 1800 model). The surface morphology of the films was examined by using a scanning electron microscopy (SEM), Model JEOL-SM-6360, Japan, operated at 20 KV. The surface wettability study was carried out on the advanced Goniometer (Model 500-F1, Rame-Hart Instrument Co. USA) at atmospheric pressure and room temperature. Cyclic voltammetry (CV) experiments were conducted at a 20 mV/s using an electrochemical analyzer (CH instruments). Hybrid films are used as a working electrode. Graphite having elemental carbon –C–C–C– is used as a counter electrode (chemical composition ash, 14.92%; volatile matter, 2.93%; and BS 200 mesh (94%)). The potential was swept between −0.5 and +0.9 V with respect to SCE in 1 M H_2SO_4 electrolyte.

Results and discussion

XPS analysis

Qualitative analysis of the electronic structures and chemical properties of the CuO-PAA and CuO-PAA/CNT films are studied by XPS. Figure 1 (a) shows the core level spectrum for the Cu2p peak over 930–970 eV corresponding to the $CPCNT_{500}$ film. The peaks observed at (1) 934.68 eV and (2) 954.90 eV, are assigned to $Cu2p_{1/2}$ and $Cu2p_{3/2}$, respectively. Additionally, two satellite peaks are observed at 944.61 and 963.16 eV that are positioned at higher binding energies as compared to the main peaks and the difference between them is found to be about 9 eV. These

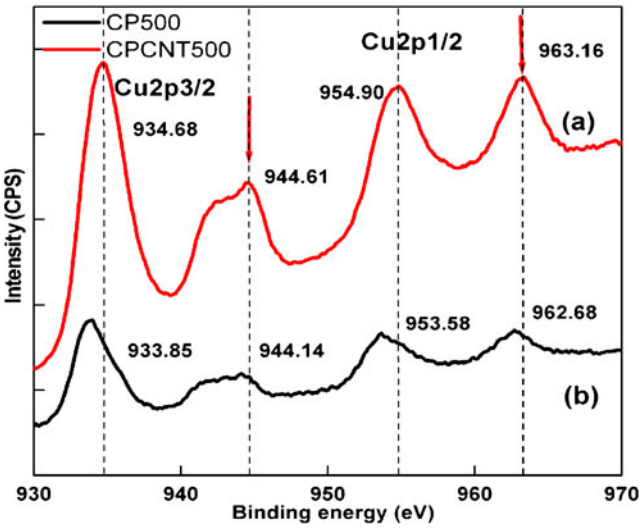

Fig. 1 The magnified view of Cu2p peak over 930-970 eV of (**a**) $CPCNT_{500}$ and (**b**) CP_{500} films

results indicate the formation of the CuO phase [22, 23]. The core level spectrum for the Cu2p peak corresponding to the CP_{500} film is shown in Fig. 1 (b). Similar to the $CPCNT_{500}$ film, two main and two satellite peaks are observed, albeit with less intensity, confirming the formation of CuO phase. However, there is a red shift about 0.5 to 1.0 eV in their binding energies indicating chemical bonding of CuO-PAA and CNT [24]. Similar results have been observed by Chusuei et al. for CuO thin films [25]. O1s core level spectrum for $CPCNT_{500}$ film de-convoluted with three components at 531.94, 533, and 530.29 eV, which are assigned to the C = O, OH, and O^{2-} (Fig. 2a). It reveals the attachment of C = O and OH groups to CuO structure. Moreover, the slight shift in O1s spectrum of $CPCNT_{500}$ is observed due to the presence of CNTs in the film (Fig. 2b).

FT-IR spectroscopy

The FT-IR spectra were recorded for the analysis and confirmation of bonding between CuO-PAA and MWCNT-COOH. Figure 3a and b represent the FT-IR spectra of pristine and functionalized MWCNTs. Four characteristic peaks at 2,939, 2,845, 1,614, and 1,450 cm^{-1} corresponds to SP^3 C–H, SP^2 C–H stretching vibrations and C = C bond are observed in both spectrum [21]. However, one more peak at 1,745 cm^{-1} in functionalized MWCNTs spectrum indicates the attachment of –COOH group to MWCNTs.

Figure 4a demonstrates the spectrum for CP_{500} film. The high-frequency modes at 532 and 592 cm^{-1} correspond to Cu–O stretching along [101] and [101] directions are observed [26]. Further, the existence of three more peaks at 1,624, 1,456, and 1,732 cm^{-1} ascertain the presence of C = C bond and COOH group of PAA. This confirms the formation of CuO-PAA hybrid film. Figure 4b–d show the FT-IR spectra of $CPCNT_{300}$, $CPCNT_{400}$, and $CPCNT_{500}$, respectively. The modifications in the spectrum of samples containing F-MWCNTs ($CPCNT_{300}$, $CPCNT_{400}$, and $CPCNT_{500}$) with respect to without F-MWCNTs sample (CP_{500}) are as (1) blue shift in Cu–O twin peak at 554 (±10) and 615 (±10)cm^{-1}, (2) blue shift in the peak located at 1,743 (±2)cm^{-1} corresponding to –COOH group. These modifications in the spectrum revealed the covalent bonding between CuO-PAA and F-MWCNTs.

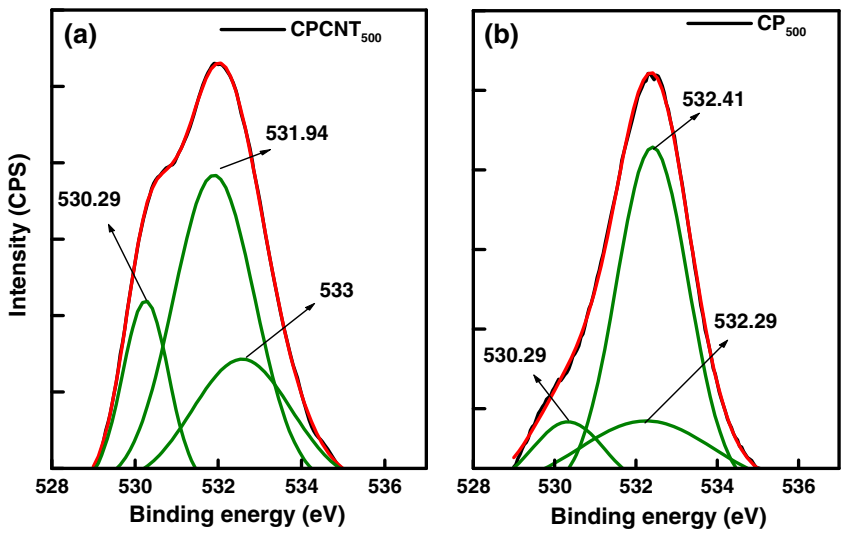

Fig. 2 The O1s core level spectra for (**a**) $CPCNT_{500}$ and (**b**) CP_{500} films

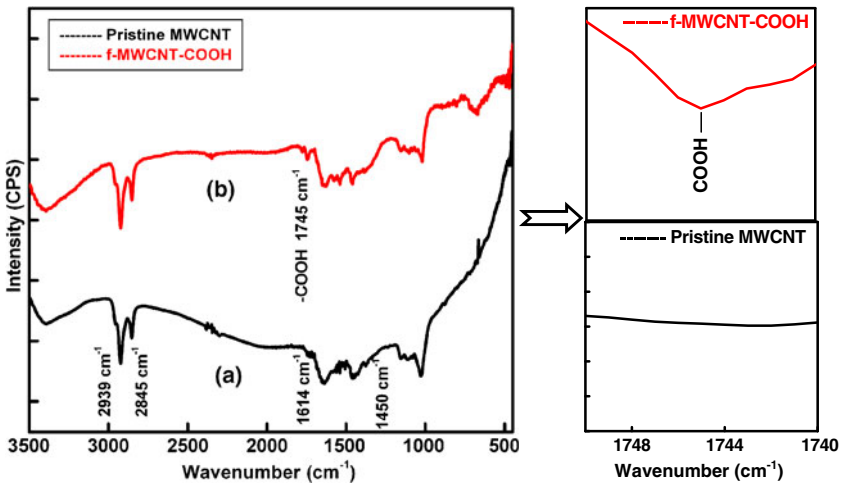

Fig. 3 FT-IR transmittance spectra for (**a** and **c**) pristine CNTs and (**b** and **d**) functionalized CNTs are recorded in the wave number range of 450-4000 cm^{-1}

Scanning electron microscopy

Figure 5a shows the SEM micrograph of the CP_{500} film. The CuO crystallites located inside the ring are surrounded by PAA grafted ring. Loosely bound PAA starts decomposing during annealing process at 500 °C and have formed CuO crystallites surrounded by PAA grafted ring with 15 μm diameter (shown in the inset). SEM micrograph of $CPCNT_{300}$ reveals that CNTs do not change the shape of the rings. However, it shrinks the size of the rings from 15 to 0.5 μm in diameter (Fig. 5b). Inset shows the magnified image of $CPCNT_{300}$ film. As the annealing temperature increased the rings are uniformly formed over the $CPCNT_{400}$ film surface (Fig. 5c). The shape of the ring remains the same but the average diameter of the rings reduced up to 600 nm as compared with CP_{500} film. $CPCNT_{500}$ also shows ring-like structure having the average diameter 1.2 μm (Fig. 5d). Hence, additions of the CNTs affect the size of ring-like structure. Zheng et al. synthesized nanomicrospheres of CuO and CuO-CNT composites by solution method. They have also observed that the CNTs do not change the shape of the nanomicrospheres of CuO [27].

Contact angle study

Figure 6a–c illustrates the variation in contact angle of $CPCNT_{300}$, $CPCNT_{400}$, and $CPCNT_{500}$ films. Surface of the films transform from hydrophobic to hydrophilic (120 to 65°) with annealing temperature. It is beneficial for improvement in the supercapacitor behavior because hydrophilic surfaces facilitate ionic diffusion process and reduces diffusion resistance of the electrolyte into electrode [28].

Cyclic voltammetry

CV measurement was employed to study the electrochemical properties of the films. The cell is configured, in a conventional three electrode cell:

$$SS/\text{hybrid film}/H_2SO_{4(aq)}/SCE/G$$

where hybrid film acts as a working electrode, saturated calomel electrode serves as a reference electrode, and

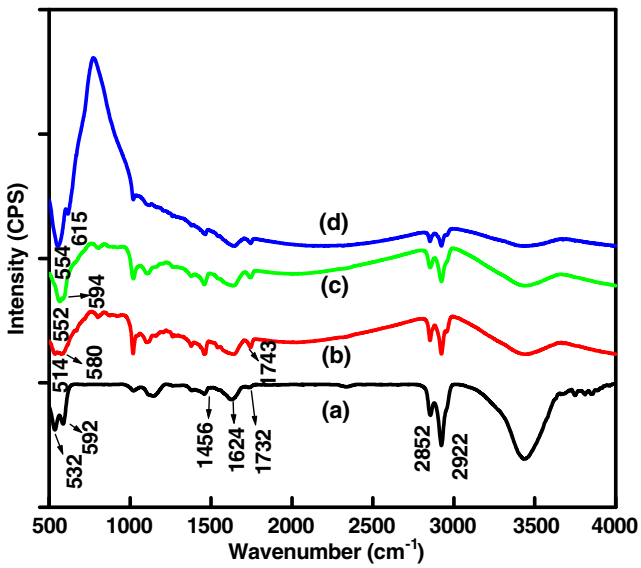

Fig. 4 FT-IR transmittance spectra for (**a**) CP_{500} sample (**b**) $CPCNT_{300}$ (**c**) $CPCNT_{400}$ and (**d**) $CPCNT_{500}$ films

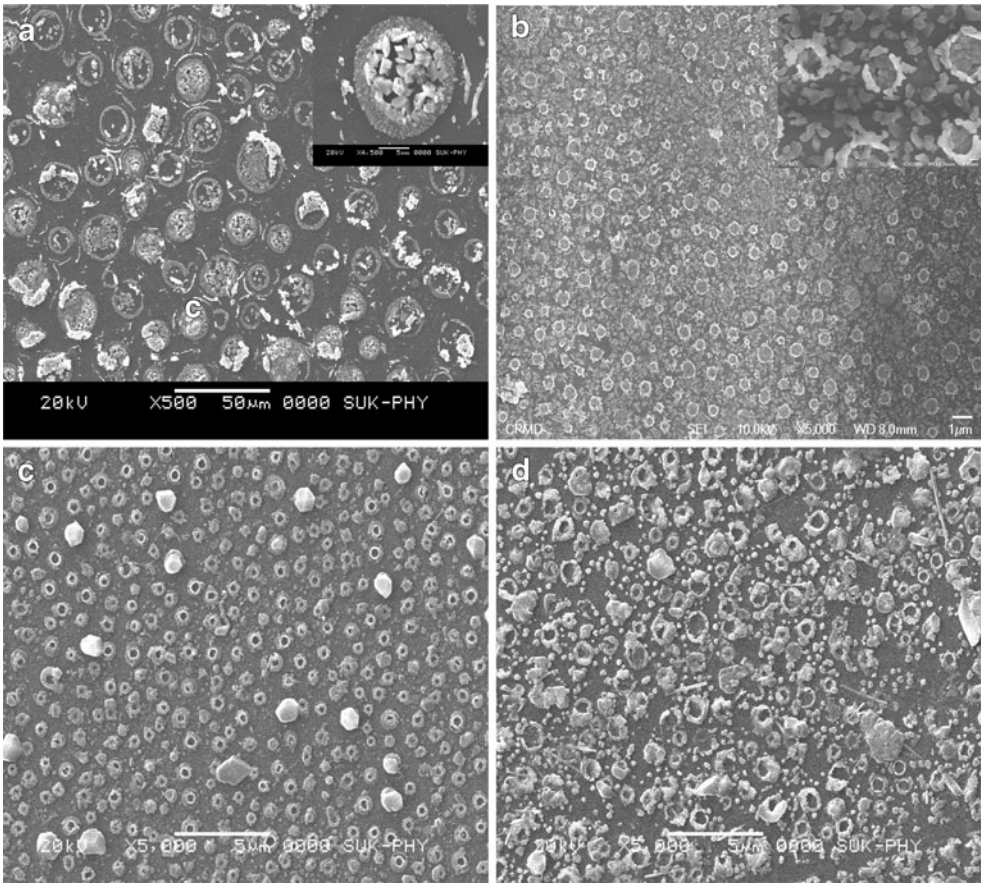

Fig. 5 SEM images of (**a**) CP_{500}; Inset shows single ring, (**b**) $CPCNT_{300}$; Inset shows magnified image, (**c**) $CPCNT_{400}$ and (**d**) $CPCNT_{500}$ samples

graphite (G) acts as a counter electrode. The average C_{sp} was calculated according to the equation:

$$C_{sp}=\frac{i}{V\times W} \quad (1)$$

where i, V, and W represent average current, scan rate, and weight of deposited hybrid films.

Figure 7 shows the CV of the CP_{500} film was swept between +0.7 and −0.4 vs. SCE in 1 M H_2SO_4. Final C_{sp} is the mean value of the C_{sp} measured using centered area of CV at 0.2, 0, and −0.2 V, respectively [29]. The calculated C_{sp} is calculated to be 136 Fg^{-1} at 20 mV/s. Figure 8 shows the overlaid CVs of $CPCNT_{300}$, $CPCNT_{400}$, and $CPCNT_{500}$ films in 1 M H_2SO_4 at 20 mV/s. C_{sp} is calculated using a similar method for $CPCNT_{300}$, $CPCNT_{400}$, and $CPCNT_{500}$ films. The peak current does not contribute much to the final C_{sp} of the films. The higher current density over large potential window in the CVs plot indicates the enhancement in the C_{sp} from 188, 220, to 258 Fg^{-1}, respectively, as compared with CP_{500}. Moreover, the redox peaks over −0.3 to 0.04 V in the CV plots can be ascribed to oxygenated groups attached to the surface of the carbon nanostructures, such as COOH [30–32]. Chidembo et al. studied the effect of acid-functionalized MWCNTs on the performance of

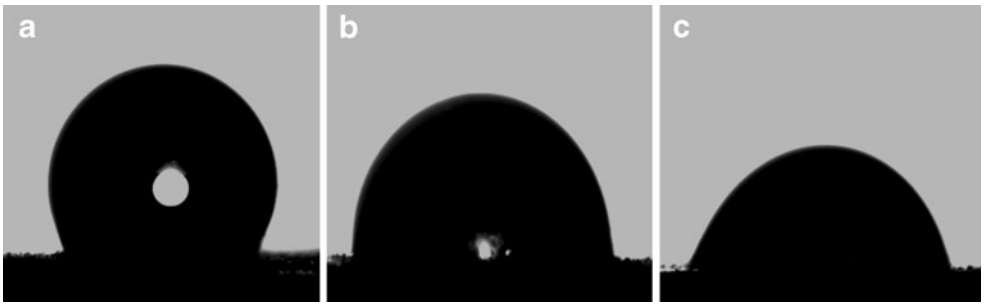

Fig. 6 The photographs of contact angle of water on the film surface of (**a**) $CPCNT_{300}$ (**b**) $CPCNT_{400}$ and (**c**) $CPCNT_{500}$ films

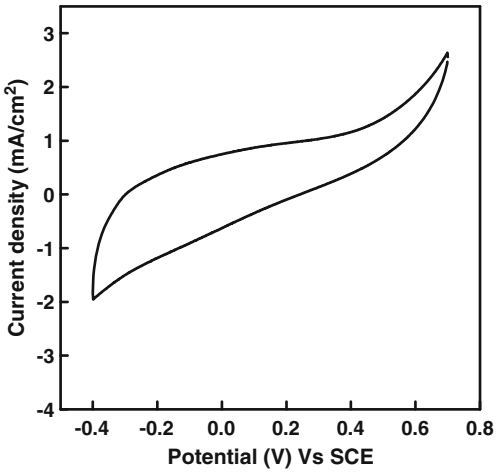

Fig. 7 CV of the CP_{500} film was swept between +0.7 to -0.4 vs SCE in 1 M H_2SO_4

nickel (II) tetraaminophthalocyanine-based supercapacitor. They reported that acid-functionalized MWCNTs are associated with surface reactions with peaks at −0.1, 0.05, and 0.2 V instead of the typical rectangular shape expected of an EDLC behavior of carbon materials as MWCNTs [31]. Pan et al. reported the tubes-in-tubes carbon nanostructures as a supercapacitor. They showed that the carbon-based supercapacitor depends on two types of accumulated energy: EDLCs and Faradic reaction-induced pseudocapacitance. The redox peaks of the CV plots over 0.2 to 0.4 V are ascribed to the oxygenated groups attached to the surface of the carbon nanotubes [32].

The reversibility of the film is also important for the development of the supercapacitor. The differences between the anodic and cathodic peak potential defines the reversibility of the film. CV of $CPCNT_{300}$ shows cathodic peak at −0.34 V and anodic peak at 0.041 V with potential difference of 0.29 V. This difference is large; hence, $CPCNT_{300}$ film is less reversible. This may be due to low wettability of the film. Similar to this, $CPCNT_{400}$ shows the cathodic and anodic peaks at −0.21 and 0.041 V causing 0.16 V potential differences. Hence, $CPCNT_{400}$ film is relatively more reversible than $CPCNT_{300}$ film. Finally, $CPCNT_{500}$ film exhibits peak in the close proximity, which reduces potential difference up to 0.043 V, indicating an improvement in the film's electrochemical reversibility. The highest C_{sp} and good reversibility over a larger potential window for $CPCNT_{500}$ film are due to increased electronic conductivity and wettability.

Two mechanisms/models are proposed for supercapacitor charge storage in CuO. The first mechanism is based on the intercalation/extraction of protons in the electrode that is oxidation/reduction of the electrode (reaction (1) in Eq. (3)), and the surface adsorption and desorption of protons (reaction (2) in Eq. (4)): When the CuO electrode is swept towards negative potential vs. SCE, the cathodic current flows owing to $Cu^{2+} \leftrightarrow Cu^{1+}$ reduction process. Similarly, during positive potential, anodic current flows due to $Cu^{1+} \leftrightarrow Cu^{2+}$ oxidation process. The following reaction represents the redox reaction in the cell:

$$Cu^{2+} + e^- \leftrightarrow Cu^+ \tag{2}$$

$$2CuO + 2H^+ + 2e^- \rightleftharpoons Cu_2O(OH) \tag{3}$$

The charge storage mechanism of CuO electrode in aqueous 1 M H2SO4 electrolyte has been proposed as follows:

$$(2CuO)_{surface} + 2H^+ + 2e^- \rightleftharpoons (Cu_2O(OH))_{surface} \tag{4}$$

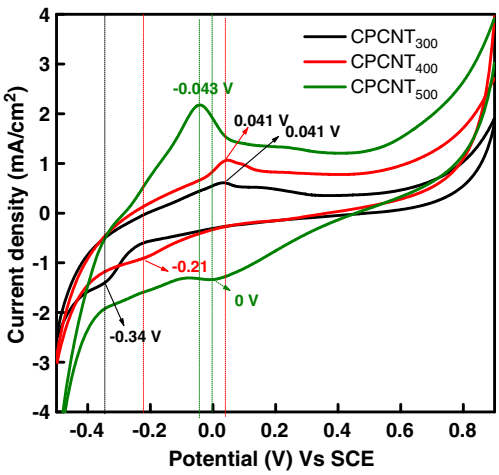

Fig. 8 CVs of the $CPCNT_{300}$, $CPCNT_{400}$ and $CPCNT_{500}$ films were swept between 0.9 to -0.5 V vs. SCE in 1 M H_2SO_4

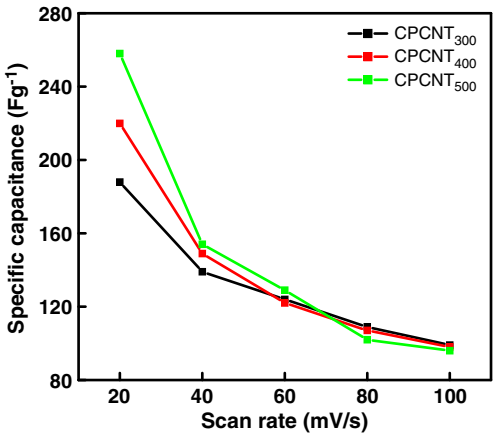

Fig. 9 The variation of the specific capacitance Vs scan rate in 1 M H_2SO_4 of (**a**) $CPCNT_{300}$ (**b**) $CPCNT_{400}$ and (**c**) $CPCNT_{500}$ films

The capacitance of carbon-based electrochemical supercapacitors depends on two kinds of accumulated energy: the electrostatic attraction in EDLCs and Faradic reaction-induced pseudocapacitance. Redox peaks in the plot indicates the existence of oxygenated groups on the surface of the MWCNTs, which leads to remarkable pseudocapacitance. Redox reaction (Faradic process) can be considered as follows:

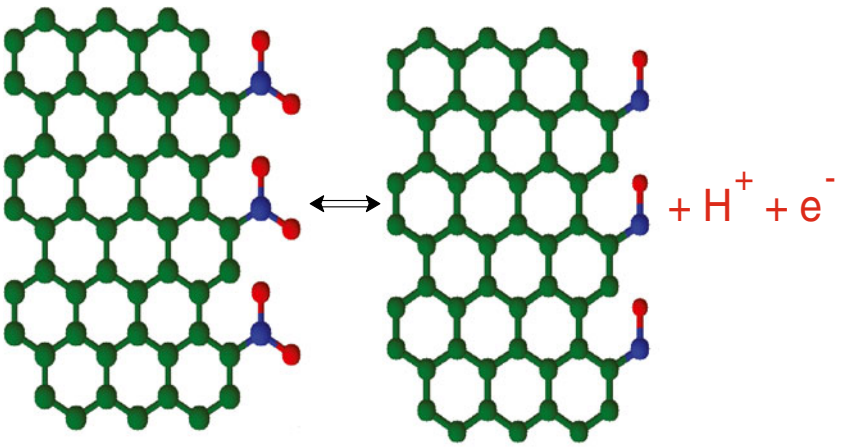

where

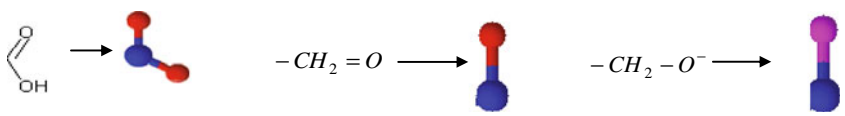

To study the effect of scan rate on the performance of supercapacitor behavior, CVs at different scan rates were recorded in 1 M H_2SO_4 electrolyte. The variation in C_{sp} Vs scan rate for $CPCNT_{300}$, $CPCNT_{400}$, and $CPCNT_{500}$ films are shown in Fig. 9 (black, red, and green). It clearly indicates that the C_{sp} decreases with increase in scan rate because the redox processes is mainly governed by insertion/desertion of the $H^{\pm}$ ions from the electrolyte into/out of the films. Increase in the scan rate impact directly on the diffusion of $H^{\pm}$ ions into the host matrix, since at higher scan rates H^{+} ions only approach the outer surface of the electrode material. Besides, the currents increase with the increase of the scan rate, indicating rapid reversible redox reaction occurred among the electrode materials.

Stability of an electrode material is important in supercapacitor. Figure 10a–c show CVs of $CPCNT_{300}$, $CPCNT_{400}$, and $CPCNT_{500}$ up to the 2,000 cycle in the voltage range of +0.7 to −0.4 vs. SCE at 20 mV/s. The inset shows the variation in C_{sp} as a function of cycle number. $CPCNT_{300}$ film exhibit decay in C_{sp} (58%) 110 Fg^{-1} up to 100 cycles with respect to C_{sp} (188 Fg^{-1}) of first cycle. However, $CPCNT_{400}$ and $CPCNT_{500}$ films exhibit 56% and 45% decrement in C_{sp} up to 100 cycles. The maximum decrement in the C_{sp} is observed in first 100 cycles, it may be due to degradation of active materials which are weakly bonded on the surface or just adsorbed on the surface. After 100 cycles, the value of C_{sp} remains almost the same. From this study, it is concluded that the stability of the CuO-PAA/CNT films increases with increase in the annealed temperature.

Conclusions

CuO-PAA/CNT hybrid films were deposited by simple and cost-effective spin-coating technique. The systematic study of annealing temperature (300 to 500 °C) on performance of CuO-PAA/CNT-based supercapacitor is studied. XPS and FT-IR analysis confirms the formation of CuO-PAA/CNT hybrid films. Novel ring-like morphology is grown for all films; however, its average diameter increases from 0.5 to 1.2 μm with annealing temperature. The C_{sp}, reversibility, and stability of the films increased substantially with increase in annealing temperature. Highest C_{sp} (258 Fg^{-1}), reversibility, and stability were observed for films annealed at 500 °C ($CPCNT_{500}$). Hence, the deposited CuO-PAA/CNT hybrid films are potential candidate for the cost-effective supercapacitor fabrication.

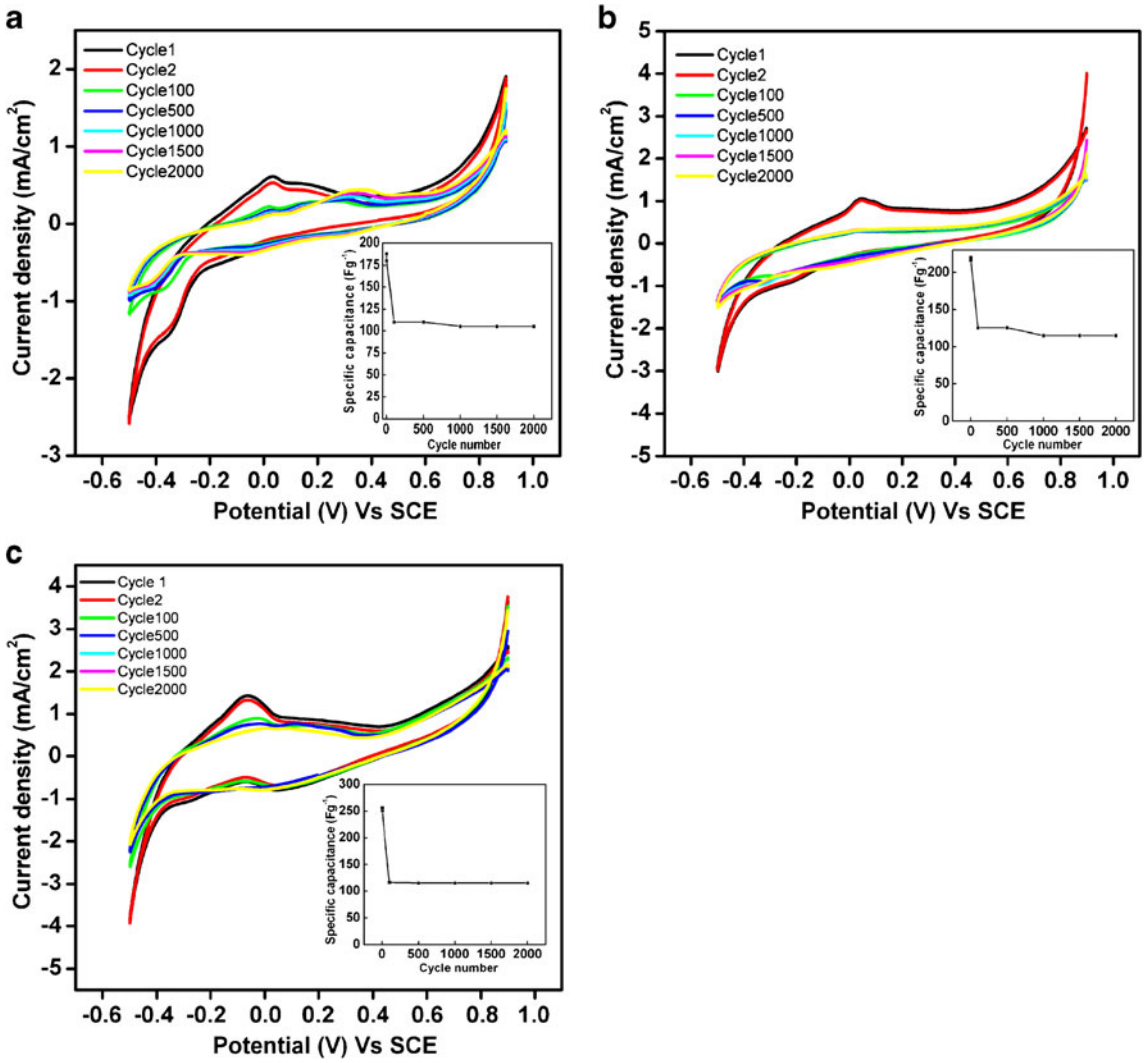

Fig. 10 The CVs of (**a**) $CPCNT_{300}$ (**b**) $CPCNT_{400}$ and (**c**) $CPCNT_{500}$ up to the 2000 cycle. Inset shows the variation of the specific capacitance of as a function of cycle number

Acknowledgments The authors are thankful to University Grants Commission, New Delhi, for the financial support through project F. no. 36-211/2008(SR) and the UGC-DRS (SAP)-II program.

References

1. Arbizzani C, Mastragostino M, Soavi F (2001) J Power Sources 100:164
2. Sharma RK, Oh HS, Shul YG, Kim H (2007) J Power Sources 173:1024
3. Liu R, Cho S, Lee SB (2008) Nanotechnology 19:215710
4. Du X, Wang C, Chen M, Jiao Y, Wang J (2009) J Phys Chem C 113:2643
5. Wang YG, Wang ZD, Xia YY (2005) Electrochim Acta 50:5646
6. Ryu KS, Kim KM, Park YJ, Park NG, Kang MG, Chang SH (2002) Solid State Ionics 152:861
7. Portet C, Taberna PL, Simon P, Flahaut E, Robert CL (2005) Electrochim Acta 50:4174
8. Frackowiak E, Beguin F (2002) Carbon 40:1775
9. Zheng JP, Cygan PJ, Jow TR (1995) J Electrochem Soc 142:2699
10. Hu CC, Huang YH (1999) J Electrochem Soc 146:2465
11. Mondal SK, Bari K, Munichandraiah N (2007) Electrochem Acta 52:3258
12. RIchard Prabhu Gnanakan S, Rajasekhar M, Subramania A (2009) Int J Electrochem Sci 4:1289
13. Mi H, Zhang X, Ye X, Yang S (2008) J Power Sources 176:403
14. Frackowiak E, Jurewicz K, Szostak K, Delpeux S, Beguin F (2002) Fuel Process Technol 77:213
15. Frackowiak E, Delpeux S, Jurewicz K, Szostak K, Cazorla-Amoros D, Beguin F (2002) Chem Phys Lett 361:35
16. Zhang LL, Zhao XS (2009) Chem Soc Rev 38:2520
17. Ko JM, Kim KM (2009) Mater Chem Phys 114:837
18. Dubal DP, Dhawale DS, Salunkhe RR, Jamdade VS, Lokhande CD (2010) J Alloys Compd 492:26
19. Reddy ALM, Ramaprabhu S (2007) J Phys Chem C 1:7727
20. Xue T, Xu CL, Zhao DD, Li XH, Li HL (2007) J Power Sources 164:953
21. Yang Z, Chen XH, Xia SZ, Pu YX, Xu XY, Li WH, Xu LS, Yi B, Pan WY (2007) J Mater Sci 42:9447
22. Tomida T, Hamaguchi K, Tunashima S, Katoh M, Masuda S (2001) Ind Eng Chem Res 40:3557
23. Poulston S, Parlett PM, Stone P, Bowker M (1996) Surf Interface Anal 24:811
24. Morales J, Espinos JP, Caballero A, Gonzalez-Elipe AR (2005) J Phys Chem B 109:7758
25. Chsuei CC, Brookshier MA, Goodman DW (1999) Langmuir 15:2806
26. Xu Y, Chen D, Jiao X (2005) J Phys Chem B 109:13561
27. Zheng SF, Hu JS, Zhong LS, Song WG, Wan LJ, Guo YG (2008) Chem Mater 20:3617
28. Conway BE (1999) Electrochemical supercapacitor: scientific fundamentals and technological application. Kluwer Academic/ Plenum Publisher, New York, p 189
29. Shaikh JS, Pawar RC, Devan RS, Ma YR, Salvi PP, Kolekar SS, Patil PS (2010) Electrochem Acta. doi:10.1016/j.electacta.2010.11.046
30. Masarapu C, Zeng HF, Hung KH, Wei B (2009) ACS Nano 3:2199
31. Chidembo AT, Ozoemena KI, Agboola BO, Gupta V, Wildgoose GG, Compton RG (2010) Energy Environ Sci 3:228
32. Pan H, Poh CK, Feng YP, Lin J (2007) Chem Mater 19:6120